NOTES AND CORRESPONDENCE

Vector Representation of Trade Cumulus Thermodynamic Fluxes

ALAN K. BETTS

*West Pawlet, VT 05775**

9 April 1985 and 3 July 1985

ABSTRACT

A vector representation of the BOMEX thermodynamic budget data is presented which shows graphically the relationship of the fluxes and the mean layer structure.

1. Introduction

The BOMEX undisturbed Tradewind budget data has already been analyzed several times (Holland and Rasmusson, 1973; Nitta and Esbensen, 1974; Betts, 1975; Nitta, 1975) and the purpose of this short paper is simply to re-express the fluxes in a simple vector format using the saturation point (SP) notation introduced by Betts (1982a). This shows very clearly the coupling of the fluxes, the changing Bowen ratio with height and suggests that given sufficiently good budget data, some information about the statistics of cloud mixing and the radiative–convective coupling can perhaps be extracted from bulk budgets.

Nitta (1975) inverted the BOMEX budget data using a spectral model which assumed lateral entrainment (Arakawa and Schubert, 1974). This technique has been widely applied in various forms to diagnostic studies of cumulus budget data (Ogura and Cho, 1973; Johnson, 1976; Houze and Leary, 1976). Betts (1975) showed that a single mass flux represented the BOMEX budget data well, and that agreement was slightly better with a nonentraining cloud model than one with lateral entrainment. Beniston and Sommeria (1981) have shown that the single mass flux parameter model is a very good fit to the fluxes predicted by a three-dimensional (3-D) simulation of a shallow cloud field. This suggests that perhaps the 3-D model statistics could be used to estimate in-cloud mixing processes. There has recently been new observational support for an old idea (Squires, 1958), namely, that cumulus clouds may entrain primarily at cloud-top (Paluch, 1978; Boatman and Auer, 1983; LaMontagne and Telford, 1983). Betts (1982a, 1983, 1984) has developed a conserved parameter representation of moist thermodynamics using air parcel *saturation point* (Betts, 1982a) which enables a simple vector representation of fluxes in terms of SP differences on a thermodynamic diagram. With this technique the extent and limitations of the information content in the thermodynamic budget data become readily visible. We shall see that the BOMEX budget data suggests some role for cloud-top entrainment, but in view of the corrections made to the humidity data, this evidence can only be regarded as encouraging for further analysis of data along these lines. We also are reminded that radiative cooling off cloud-tops may play an important role in the budgets.

2. Parametric model

Following Betts (1975), we may express the fluxes in the tradewind layer of the product as a mass flux (ω^*/g) and a cloud–environment difference ($\mathbf{C} - \mathbf{E}$).

$$g\mathbf{F}(p) = \omega^*(p)[\mathbf{C}(p) - \mathbf{E}(p)]. \tag{1}$$

We use a vector notation where **C**, **E** are representative SPs for a cloud, and environment parcel (Betts, 1984). In general, **C** and **E** vary with height. For a small fractional cloud cover, $\mathbf{E}(p)$ is closely the mean stratification, while the variation of $\mathbf{C}(p)$ will depend on the cloud–environment mixing processes. If there is no mixing, then **C** stays at **B**, the SP of air ascending through cloud-base, which is closely the SP of the nearly well mixed subcloud layer. In the budget method we generally know **E** and **F**. What can be determined about convective mass flux ω^* and the mean cloud SP, **C**? Since ω^* is a scalar, the flux vector **F** has the same vector orientation as the difference $\Delta\mathbf{S} = \mathbf{C} - \mathbf{E}$. If we consider $\Delta\mathbf{S}$ to have components $\Delta\theta_l$, Δq_t, then the ratio of the conserved heat flux to the total water flux is

$$\mathrm{BR} = c_p\Delta\theta_l/L\Delta q_t \tag{2a}$$

where BR is the Bowen ratio for the conserved fluxes (Betts, 1984). In parameterizing the flux data we shall approximate static energy differences with the differences $c_p\Delta\theta$. Thus, we can determine the orientation of $\mathbf{C} - \mathbf{E}$ on a thermodynamic diagram directly from the

* Visiting scientist, NASA-Goddard Space Flight Center, Code 613, Greenbelt, MD 20771.

© 1985 American Meteorological Society

flux data without knowing ω^*. This gives a hint of the cloud–environment mixing process because cloud-top and lateral entrainment rotate the vector (**C** − **E**) differently with height (see Section 3).

3. Data

Table 1 shows the mean structure and fluxes for a 3-day averaged dataset (22–24 June 1969) for the BOMEX ship array (data supplied by E. Rasmusson). The flux data was computed by integrating the heat and moisture budgets downwards from $\hat{p} = 300$ mb ($\hat{p}$ is pressure, $p_0 - p$, below the surface pressure, $p_0 \approx 1016$ mb). The first two columns show the fluxes of liquid water static energy (s_l) and total water (q_t). They are very similar to those in Betts (1975), Fig. 1. The third column is the ratio of these fluxes, the Bowen ratio

$$\mathrm{BR} = \mathbf{F}_{s_l}/\mathbf{F}_{Lq_t}. \tag{2b}$$

Conventionally, this is only defined at the surface, but it is convenient to call this ratio of the conserved fluxes, the flux Bowen ratio at any level. Betts (1984) showed how the orientation of a flux vector, parameterized in terms of Eq. (1), rotates with the Bowen ratio given by (2). The fourth and fifth column show the Bowen ratio associated with the vector (**C** − **E**) in (1) computed for two different assumptions on **C**. The first, labeled $\beta = 0$, corresponds to no mixing and assumes the typical cloud **C** does not change from the cloud-base SP, **B** (computed as a subcloud layer mean). Betts (1975) showed that this parameterization

$$g\mathbf{F} = \omega^*(\mathbf{B} - \mathbf{E}) \tag{3}$$

gives a reasonable fit to the BOMEX flux data. Table 1 confirms this. The values and trend of Bowen ratio with $\hat{p}$ are similar for this "no mixing" model and the flux data (columns 4 and 5). The differences at cloud-base ($\hat{p} = 60$ mb) are very sensitive to small errors in **B** or $\mathbf{F}_{s_l}$, and there is some divergence above $\hat{p} = 160$ mb, which is the Trade inversion layer (see below). The sixth column shows (**C** − **E**) computed assuming cloud-top mixing parameterized as in Betts (1982b), so that the typical cloud parcel saturation level p^* moves up the mixing line between cloud-base and cloud-top air as pressure changes at a rate

$$\beta = dp^*/dp = 0.3. \tag{4}$$

The corresponding Bowen ratios are a somewhat better fit to the flux data (columns 4 and 6), although above $\hat{p} = 160$ mb the agreement is again poor.

Fig. 1 shows the flux data graphically on a Tephigram. The solid circles are the SPs of the mean sounding (labeled with their $\hat{p}$ level). The arrows indicate the direction and relative magnitude of the flux vectors at the corresponding $\hat{p}$ levels. The arrows have been normalized so that the cloud-base flux vector is represented by (**B** − **E**) at cloud-base: this is equivalent to computing from (1) a vector (**C** − **E**) using the cloud-base mass flux. The dotted continuation of these flux arrows show where they intersect the cloud-top mixing line (heavy dashes). This rotation of the flux vectors counterclockwise from the vector (**B** − **E**) confirms that the observed fluxes are consistent with some cloud-top mixing which would move cloud parcel SP **C** up the mixing line **BT**. In contrast, lateral entrainment would rotate the flux vectors clockwise relative to [**B** − **E**($\hat{p}$)] by moving **C**($\hat{p}$) from **B** towards the environmental SP profile. (For example, for lateral entrainment **C**($\hat{p} = 100$) might be modelled by some average of **B** and **E**[$\hat{p} = 80$)]. These flux vector rotations are small and in view of the corrections to the humidity data in the BOMEX dataset, this should be regarded as only an indication of the presence of cloud-top mixing.

Although this analysis couples the convective fluxes through ω^*/g, we can see that the flux data do not

TABLE 1. Undisturbed BOMEX budget (22–24 June 1969). Profiles of conserved thermodynamic fluxes and flux Bowen ratio from budget, and Bowen ratio and convective mass flux computed from cloud model. Cloud-base is at $\hat{p} = 60$mb.

	Flux data		Bowen ratio			
				Model		
$\hat{p}$ (mb)	F_{s_l}	F_{Lq_t}	Flux	$\beta = 0$ (no mixing)	$\beta = 0.3$ (cloud-top mixing)	Computed ω^*/g for $\beta = 0.3$ ($\times 10^{-3}$ Kg m^{-2} s^{-1})
	(W m^{-2})					
0	18	189	0.10			
20	12	185	0.07			
40	5	180	0.03			
60	−3	172	−0.02	−0.04	−0.04	94
80	−10	161	−0.06	−0.10	−0.07	33
100	−15	148	−0.10	−0.15	−0.12	20
120	−20	135	−0.15	−0.18	−0.15	15
140	−25	126	−0.20	−0.22	−0.19	13
160	−28	111	−0.25	−0.24	−0.22	10
180	−24	69	−0.35	−0.25	−0.24	4
200	−14	19	−0.74	−0.27	−0.26	1
220	−6	0				

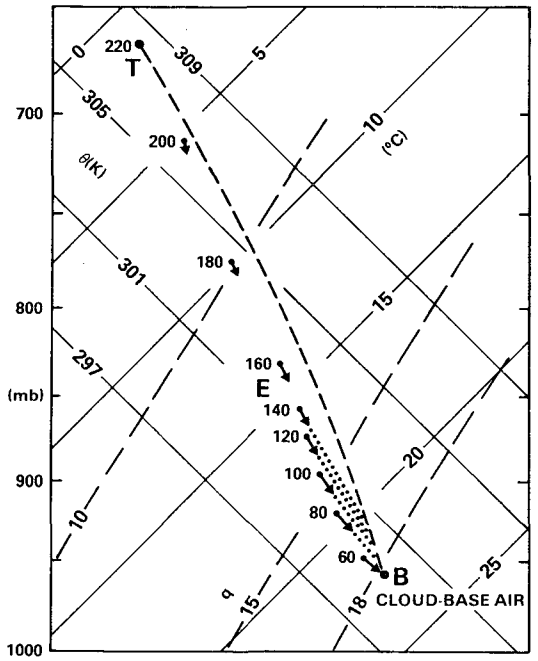

FIG. 1. Tephigram showing BOMEX averaged thermodynamic flux vectors (22–24 June 1969) as arrows, the mixing line (heavy dashes) between cloud-base and cloud-top saturation points **B** and **T**, and the mean environmental (**E**) saturation points (solid circles) labelled with their pressure levels (as a difference from the surface pressure).

give us a unique solution for the convective mass flux. If we *assume* cloud-top mixing so that $\mathbf{C}(\hat{p})$ follows the heavy dashed mixing line in Fig. 1, then ω^*/g can be computed from this specific cloud model. The last column in Table 1 shows ω^*/g, decreasing with height, computed with $\beta = 0.3$ from the q_t flux. The shape is similar to the profiles in Betts (1975), although the values are considerably larger because of larger corrections to the humidity data.

However, Fig. 1 shows that, although cloud-parcel $\mathbf{C}(\hat{p})$ is constrained, it cannot be determined uniquely from the flux data. For example, at any $\hat{p}$, $\mathbf{C}(\hat{p})$ might be anywhere along the dotted line between $\mathbf{E}(\hat{p})$ and the cloud-top mixing line, with a correspondingly larger value of ω^* larger than in Table 1. (This would require lateral as well as cloud-top mixing.)

Above $\hat{p} = 160$ mb, the flux vectors rotate clockwise. Assuming this is not simply data error, it could reflect stronger mixing in the inversion layer. However, radiative cooling of cloud-tops will tend to cool cloud parcel **C** at constant q, and this also may produce a significant clockwise rotation of the $(\mathbf{C} - \mathbf{E})$ vector to give the larger negative Bowen ratios shown in Table 1 at $\hat{p} = 180$–200 mb.

4. Conclusions

We have presented a vector representation of the BOMEX trade cumulus budget results which shows graphically the information contained in the two independent budgets. The budgets indicate that cloud-top entrainment into active cumulus clouds may play a significant role in the transport process, but that a detailed estimate of the relative importance of cloud-top and lateral entrainment cannot be made from flux data. However, because of the considerable corrections to the BOMEX humidity data, and the inherent (but unknown) inaccuracies in the budget method itself, this conclusion can only be regarded as tentative. Nonetheless, the analysis method itself is of interest. It could also be a useful way of presenting fluxes measured directly inside cumulus or stratocumulus layers because it intercompares the flux structure, the mean profile structure, and provides at least some information on the mixing and radiative processes in the layer.

Acknowledgments. This work has been supported by the National Science Foundation, Global Atmospheric Research Program under grant ATM-8403333, and the National Aeronautics and Space Administration under contract NAS5-28590.

REFERENCES

Arakawa, A., and W. Schubert, 1974: Interaction of a cumulus cloud ensemble with the large-scale environment: Part I. *J. Atmos. Sci.*, **31**, 674–701.

Beniston, M. G., and E. Sommeria, 1981: Use of a detailed Planetary Boundary Layer Model for parameterization purposes, *J. Atmos. Sci.*, **38**, 780–797.

Betts, A. K., 1975: Parametric interpretation of trade-wind cumulus budget studies. *J. Atmos. Sci.*, **32**, 1934–1945.

——, 1982a: Saturation point analysis of moist convective overturning. *J. Atmos. Sci.*, **39**, 1484–1505.

——, 1982b: Cloud thermodynamic models in saturation point coordinates. *J. Atmos. Sci.*, **39**, 2182–2191.

——, 1983: Thermodynamics of mixed stratocumulus layers: saturation point budgets. *J. Atmos. Sci.*, **40**, 2655–2670.

——, 1984: Boundary layer thermodynamics of a high plains severe storm. *Mon. Wea. Rev.*, **112**, 2199–2211.

Boatman, J. F., and A. H. Auer, 1983: The role of cloud-top entrainment in cumulus clouds. *J. Atmos. Sci.*, **40**, 1517–1534.

Holland, J. Z., and E. M. Rasmusson, 1973: Measurements of the atmospheric mass, energy and momentum budgets over a 500-kilometer square of tropical ocean, *Mon. Wea. Rev.*, **101**, 44–55.

Houze, R. A., and C. A. Leary. 1976: Comparison of convective mass and heat transports in tropical easterly waves computed by 2 methods. *J. Atmos. Sci.*, **33**, 424–429.

Johnson, R. H., 1976: The role of convective-scale precipitation downdrafts in tropical easterly waves computed by 2 methods. *J. Atmos. Sci.*, **33**, 424–429.

LaMontagne, R. G., and J. W. Telford, 1983: Cloud-top mixing in small cumuli. *J. Atmos. Sci.*, **40**, 2148–2156.

Nitta, T., 1975: Observational determination of cloud mass flux distributions, *J. Atmos. Sci.*, **32**, 73–91.

——, and S. Esbensen, 1974: Heat and moisture budgets using BOMEX data. *Mon. Wea. Rev.*, **102**, 17–28.

Ogura, Y., and H. R. Cho, 1973: Diagnostic determination of cumulus cloud populations from observed large-scale variables. *J. Atmos. Sci.*, **30**, 1276–1286.

Paluch, I. R., 1979: The entrainment mechanism in Colorado cumuli. *J. Atmos. Sci.*, **36**, 2467–2478.

Squires, P., 1958: Penetrative downdraft in cumuli. *Tellus*, **10**, 381–389.